

<https://doi.org/10.1038/s41534-024-00824-x>

# Simulating photosynthetic energy transport on a photonic network

Check for updates

Hao Tang<sup>1,6</sup>, Xiao-Wen Shang<sup>1,6</sup>, Zi-Yu Shi<sup>1</sup>, Tian-Shen He<sup>1</sup>, Zhen Feng<sup>1</sup>, Tian-Yu Wang<sup>1</sup>, Ruoxi Shi<sup>1</sup>, Hui-Ming Wang<sup>1</sup>, Xi Tan<sup>1</sup>, Xiao-Yun Xu<sup>1</sup>, Yao Wang<sup>1</sup>, Jun Gao<sup>1</sup>, M. S. Kim<sup>2,3</sup> & Xian-Min Jin<sup>1,4,5</sup>✉

Quantum effects in photosynthetic energy transport in nature, especially for the typical Fenna-Matthews-Olson (FMO) complexes, are extensively studied in quantum biology. Such energy transport processes can be investigated as open quantum systems that blend the quantum coherence and environmental noise, and have been experimentally simulated on a few quantum devices. However, the existing experiments always lack a solid quantum simulation for the FMO energy transport due to their constraints to map a variety of issues in actual FMO complexes that have rich biological meanings. Here we successfully map the full coupling profile of the seven-site FMO structure by comprehensive characterisation and precise control of the evanescent coupling of the three-dimensional waveguide array. By applying a stochastic dynamical modulation on each waveguide, we introduce the base site energy and the dephasing term in coloured noise to faithfully simulate the power spectral density of the FMO complexes. We show our photonic model well interprets the phenomena including reorganisation energy, vibrational assistance, exciton transfer and energy localisation. We further experimentally demonstrate the existence of an optimal transport efficiency at certain dephasing strength, providing a window to closely investigate environment-assisted quantum transport.

Since experimental evidences for quantum coherent energy transport have been successively observed in many pigment-protein complexes<sup>1–4</sup>, the photosynthetic light-harvesting process began to be investigated as open quantum systems that blend the quantum coherence and environment noise<sup>5–10</sup>. The theory on environment-assisted quantum transport (ENAQT)<sup>11</sup> was then raised to suggest the enhancement of energy transport efficiencies by environment noise in many nanoscale transport systems. The ENAQT theory has been extensively studied and showed good interpretability on energy transfer among many coherent and incoherent theories<sup>12,13</sup>. The ENAQT theory has now been applied to a rich range of research areas including light-harvesting phenomena in nature, the solar cell engineering and other novel biotic excitonic devices<sup>14</sup>.

One of the most well-studied natural creatures for its light-harvesting process is the green-sulphur bacteria, since its structure is simple but highly effective to allow for enough harvest of energy from the

very dark deep sea environment<sup>15</sup>. The bacteria collect light through their large chlorosome antenna and transfer excitons to their reaction center. The cable connecting these two part is the so-called Fenna-Matthews-Olson (FMO) complex<sup>16</sup>, which is normally formed in a trimer of three complexes with each one consisting of eight bacteriochlorophyll-a (BChl-a) molecules<sup>10</sup>. Seven of the eight molecules are bound within a protein scaffold, which forms the environment for the complexes and provides the source of noise and decoherence. The eighth BChl outside the protein scaffold assists the transport of the excitation into the seven-site structure<sup>17</sup>, where the seven BChls are conventionally numbered from No. 1 to 7 (Fig. 1a). The seven-site FMO complex is a prevalent structure for the exciton transfer process. The excitation energy normally transports from BChl 1 or BChl 6 all the way to BChl 3, and eventually goes to the reaction center to accomplish the energy conversion reactions for photosynthesis.

<sup>1</sup>Center for Integrated Quantum Information Technologies (IQIT), School of Physics and Astronomy and State Key Laboratory of Advanced Optical Communication Systems and Networks, Shanghai Jiao Tong University, Shanghai 200240, China. <sup>2</sup>Blackett Laboratory, Imperial College London, London SW7 2AZ, UK. <sup>3</sup>Korea Institute of Advanced Study, Dongdaemooon-Gu, Seoul 02455, South Korea. <sup>4</sup>Chip Hub for Integrated Photonics Xplore (CHIPX), Shanghai Jiao Tong University, Wuxi 214000, China. <sup>5</sup>TuringQ Co. Ltd., Shanghai 200240, China. <sup>6</sup>These authors contributed equally: Hao Tang, Xiao-Wen Shang.

✉ e-mail: [xianmin.jin@sjtu.edu.cn](mailto:xianmin.jin@sjtu.edu.cn)

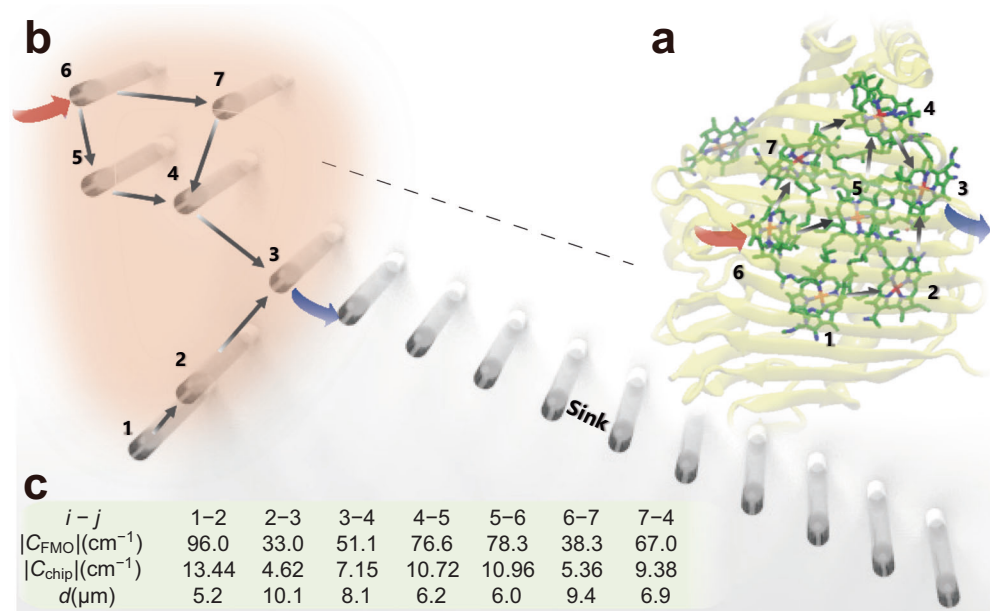


**Fig. 1 | Experimental layout.** Schematic diagram of (a) the FMO complex (Protein Data Bank accession 3ENI, image of 3BSD<sup>58</sup> created with VMD<sup>59</sup>) and (b) the three-dimensional photonic waveguide array simulating the FMO complex. The numbers of the 7 sites in the FMO complex and their corresponding waveguide are marked. The arrows show that the energy comes into the FMO complex or the waveguide array from Site 6 and moves through Site 3 to the sinks. c The absolute values of the coupling coefficient in the FMO complex of *C. tepidum*,  $C_{\text{FMO}}$  (unit:  $\text{cm}^{-1}$ ), according to<sup>40,41</sup>. In order to map  $C_{\text{FMO}}$  onto the photonic lattice of a suitable

propagation length,  $C_{\text{chip}}$  (unit:  $\text{cm}^{-1}$ ), all the coupling coefficients on chip, are proportionally reduced to 14% of  $C_{\text{FMO}}$ , which only affects the overall evolution time, but not the coupling profile among the seven sites.  $d$  (unit:  $\mu\text{m}$ ) is the center-to-center waveguide spacing between two waveguides. Such  $d$  values are set to generate the expected  $C_{\text{chip}}$  values above, as  $C_{\text{chip}}$  exponentially decays with  $d$ , which has been fitted by:  $C = 47.19 \times e^{-0.2243d}$ . The coupling coefficients between other sites are much weaker (below  $15 \text{ cm}^{-1}$ ), causing very marginal influences on the evolution pattern, and hence are not shown in the table.

Theoretical quantum physicists have investigated the FMO structure<sup>6-10</sup> and proven that there exists certain optimal environmental noise levels to assist for an optimal energy transport efficiency. In recent years, many experimental simulations for ENQAT, especially in the context of a photosynthetic complex model, have emerged<sup>18-23</sup>. They are implemented in different systems, including a programmable nanophotonic processor with discrete-time evolution<sup>19</sup>, superconducting circuits<sup>20</sup>, the nuclear magnetic resonance<sup>21</sup>, and the ion-trap qubits<sup>23</sup>, with a key goal on introducing controllable environmental noise into the original quantum system<sup>24</sup>. However, there lacks a solid mapping to the FMO photosynthetic energy transport due to various constraints. Firstly, the quantum simulator hardware did not load the full Hamiltonian matrix for the authentic FMO in nature, since simulating the coupling profile for the seven BChls demands strong capabilities on setting the two-dimensional coupling space and flexibly tuning the coupling strength. Secondly, the issue on noise for FMO was not addressed. Some studies simply use white noise<sup>18-20</sup>, while some analyze coloured noise<sup>21,23</sup>, which still does not match a spectral density for real FMO. Thirdly, there are many up-to-date works on photosynthetic energy transport<sup>25-27</sup>. Many important issues like the reorganisation energy dynamics and the assistance by vibrational coherence<sup>28-32</sup> are left for further investigations.

In this work, we present a close investigation on simulating photosynthetic energy transport in our three-dimensional photonic lattice. We map the full coupling profile of the seven-site FMO structure on a physical quantum simulator. Besides, by implementing the  $\Delta\beta$  photonic model<sup>33-36</sup>, we introduce independently controllable noise for each waveguide, which allows us to load the site energy and the coloured noise that yields a spectral density consistent with that for the actual FMO complex. We demonstrate the photonic model can simulate important biological issues including the reorganisation energy and the vibrational assistance. Furthermore, by mapping the Hamiltonian matrix and coloured noise for FMO on our photonic lattice, we carry out a quantum simulation experiment and demonstrate that an optimal energy transport efficiency exists at a certain

noise amplitude. Our work provides a window to closely investigate environment-assisted quantum transport, and may inspire further explorations on comprehensive mechanisms for light-harvesting photosynthesis.

## Results

Three-dimensional photonic array provides a highly versatile platform for quantum simulation. The longitudinal direction corresponds to the evolution time and the cross-section of the array structure could be engineered to implement a designed Hamiltonian matrix. Photons propagating through an array of  $N$  coupled waveguides can be described by a  $N \times N$  Hamiltonian matrix:

$$H = \sum_i^N \beta_i a_i^\dagger a_i + \sum_{j \neq i}^N C_{i,j} (a_i^\dagger a_j + a_j^\dagger a_i), \quad (1)$$

where the diagonal values of  $H$  are  $\beta_i$ , the propagating constant along the  $i$ th waveguide, and the off-diagonal terms are  $C_{i,j}$ , the coupling coefficient between waveguide  $i$  and  $j$ .

We use seven waveguides to represent the seven sites of the FMO complex (See Fig. 1a, b). Since the coupling coefficients between two adjacent waveguides,  $C_{\text{chip}}$ , are characterised to follow an exponential decay with the center-to-center waveguide spacing  $d$ <sup>37-39</sup>, we are able to quantitatively control  $C_{\text{chip}}$  by carefully designing the waveguide configuration (See Fig. 1c). Therefore, utilizing the two-dimensional evolution space, we faithfully map the major coupling coefficients for the real seven-site FMO complex of *C. tepidum*<sup>40,41</sup> on chip. The full information on the Hamiltonian matrix for the FMO molecule is given in Supplementary Note 1. An extra array of 100 waveguides is connected to Waveguide 3 to serve as the sink, resembling the light transport from Site 3 of the FMO complex to its reaction center (Fig. 1b).

### $\Delta\beta$ photonic approach

Our photonic array is essentially a quantum evolution system for pure quantum walks, if all propagation constants  $\beta_i$ s in Eq. (1) remain constant in time. Here we manage to modulate the diagonal term of the Hamiltonian by introducing  $\Delta\beta$ , the detunings of the propagation constant  $\beta$ , in order to create a fluctuation of the site energy<sup>33–36</sup> (Fig. 2a). A large number of stochastic  $\Delta\beta$  detunings constitute the quantum stochastic walk<sup>36</sup> and faithfully implement the dephasing process in the open quantum systems<sup>11,34</sup>. The introduction of  $\Delta\beta$  can be experimentally achieved by tuning the laser writing speed during the waveguide fabrication process (see details in Supplementary Note 2). The existence of  $\Delta\beta$  also causes some fluctuations of the effective coupling coefficient denoted as  $\Delta C$ , but the value is minor and it is shown to have very marginal influence on the transport efficiency. We hence mainly consider the model with only diagonal  $\Delta\beta$  terms (see discussions on  $\Delta C$  in Supplementary Note 3).

Using this photonic model, consider the case where each waveguide is broken up into many segments. We then have an effective piecewise dependent Hamiltonian:

$$H_{\text{eff}}(t_n) = \sum_i^N (\beta_{i0} + \Delta\beta_i(t_n)) a_i^\dagger a_i + \sum_{j \neq i}^N C_{i,j} (a_i^\dagger a_j + a_j^\dagger a_i), \quad (2)$$

where  $\beta_{i0}$  is the base propagation constant for waveguide  $i$ , and  $\Delta\beta_i(t_n)$  is the extra detunings at segment  $t_n$ . Then we have the wavefunction:  $\Psi(t_n) = e^{-iH_{\text{eff}}(t_n)\Delta t} \Psi(t_{n-1})$ , where  $\Delta t$  is the time interval for segment  $t_n$ .

Such an effective Hamiltonian  $H_{\text{eff}}$  can be straightforwardly mapped to the real modulation in segments of the photonic lattice. As shown in Fig. 2a, we set the waveguide into segments of equal length with  $\Delta t$  to be 1 mm, and we introduce various random  $\Delta\beta$  values ranging between 0 and a given amplitude denoted by  $\Delta\beta_A$ . At the end of the waveguide, measuring the light intensity distribution gives  $|\Psi|^2$ .

In this experiment-friendly photonic model, we are able to introduce the noise consistent with the actual FMO complex. Instead of plain white noise, the biological energy transport involves coloured noise that exhibits a non-Markovian nature<sup>31</sup>. Fig. 2b shows an example on the  $\Delta\beta$  values at Waveguide 7 that yield coloured noise for BChl 7 (see details on generating

white and coloured noise in Supplementary Note 4 and 5). Besides, the base site energy for the seven BChls in FMO varies. In order to reflect that, we additionally consider different base values of  $\beta_i$  for the seven waveguides representing the seven sites, as shown in Fig. 2c.

### Power spectral density

According to Wiener–Khinchin theorem, the power spectral density  $J_i(\omega)$  is the Fourier transform of the original correlation function of the signal. In the context of the  $\Delta\beta$  photonic model, it is

$$J_i(\omega) = \int_{-\infty}^{+\infty} d\tau e^{-i\omega\tau} \langle \Delta\beta_i(\tau) \Delta\beta_i(0) \rangle. \quad (3)$$

In Fig. 3a, the red bars show the pattern of the intermolecular spectral density for BChl 7 of the actual FMO complex<sup>29,30</sup>. The spectral density is obtained via normal mode analysis of the whole pigment-protein complex with the charge density coupling method for the local optical transition energies of the pigments by Klinger et al.<sup>30</sup>. It shows that the noise power for actual FMO complexes is concentrated in the low-frequency components, with some fluctuations in the mid-frequency region, and converges to 0 in the high-frequency region. Note that a hypothesis on site-independent spectral density is adopted for simplicity<sup>25</sup>, and the distributions of power spectral density at the other six sites are in similar patterns<sup>30</sup>.

The blue shading area in Fig. 3a represents the power spectral density for Waveguide 7 we generate using the coloured noise via  $\Delta\beta$  detunings. It matches the normalized pattern for actual FMO complex in terms of the shape on concentrating in low-frequency components. On the other hand, in the inset of Fig. 3a we show a distinct pattern generated from the white noise. The white noise is actually Markovian while the coloured noise exhibits strong non-Markovianity that does exist in the FMO complex<sup>31,42</sup>. See details on noise characteristics in Supplementary Note 6.

### Reorganisation energy

The photoexcitation is always accompanied by another energy transfer process. After the FMO complex is photoexcited to a localized excited state, the nuclei inside will undergo a relaxation process to achieve a new equilibrium position. The energy released during relaxation is characterised by the

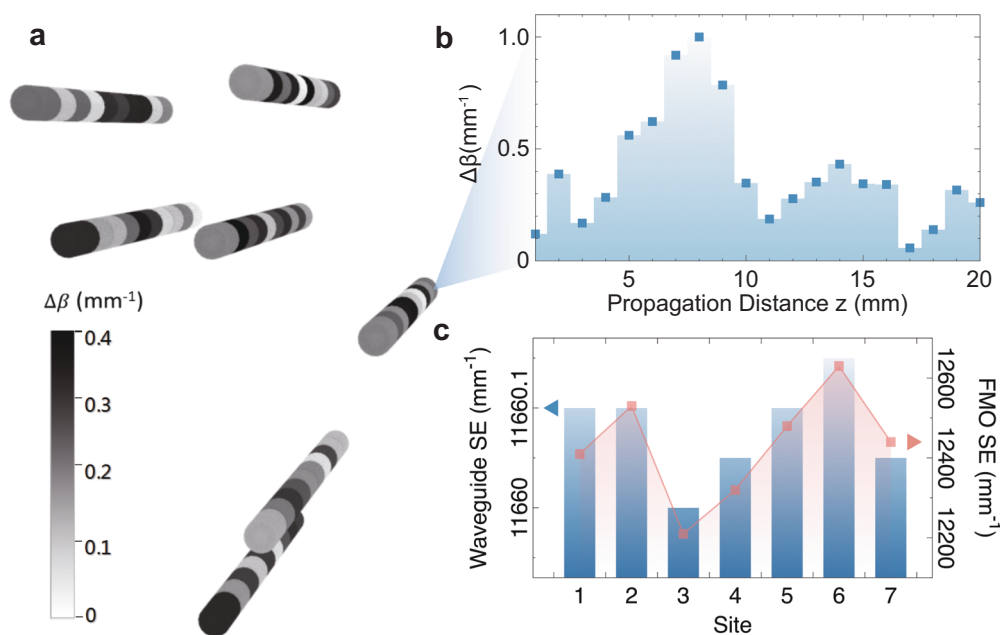


**Fig. 2 | The  $\Delta\beta$  photonic model.** **a** Schematic diagram of the randomly varying propagation constants shown in different grayscales along the propagation direction of the seven-site structure. This set of random values is one example of the cases with

a  $\Delta\beta_A$  of  $0.4 \text{ mm}^{-1}$ . **b** The arrangement for the coloured noise by the  $\Delta\beta$  detuning for one site. **c** The site energies (SE) for the seven sites of FMO and the base  $\Delta\beta$  detuning used for the seven waveguides to match the site energies.

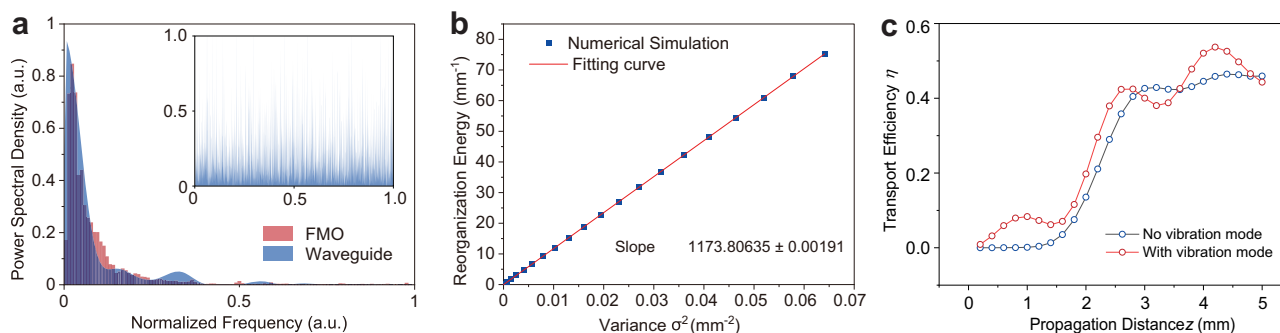


**Fig. 3 | Photosynthetic energy transport using the  $\Delta\beta$  photonic model.** **a** The spectral density formed by the coloured noise introduced on Waveguide 3 is shown in the blue shadow. The red bars show the power spectral density for BChl 3 in a pigments of the monomeric subunits of the FMO protein via normal mode analysis from Ref. 30. Inset shows a spectral density generated from the white noise. **b** Reorganisation energy versus noise variance at Site 7. The sampling frequency and

period are  $f_s = 1 \text{ mm}^{-1}$  and  $t_c = 20 \text{ mm}$ , respectively. The variance  $\sigma^2(\Delta\beta_7) = \langle(\Delta\beta_7)^2\rangle - \langle\Delta\beta_7\rangle^2$  depends on  $\Delta\beta_7$  amplitude  $\Delta\beta_{A,7}$ . The parameters of the linear fitting are given in the bottom right of the figure. **c** The transport efficiency at an early transport length with (red) and without (blue) vibrational assistance.  $\Delta\beta_A$  for all waveguides are set to be  $0.5 \text{ mm}^{-1}$ .

reorganisation energy  $E_i^{R25,27}$ , which generally indicates the strength of system-bath coupling<sup>27</sup>.  $E_i^R$  for each single site  $i$  can be calculated by:

$$E_i^R = \frac{1}{\pi} \int_0^\infty d\omega \frac{J_i(\omega)}{\omega}. \quad (4)$$

In the FMO complex, the reorganisation energy follows a quantitative relationship with the variance of noise  $\sigma^{228}$ . For site  $i$ , there is

$$\sigma_i^2 = 2k_B T E_i^R, \quad (5)$$

where  $k_B$  is the Boltzmann constant. In our  $\Delta\beta$  photonic model,  $\sigma^2(\Delta\beta_i) = \Delta\beta_i^2 - \overline{\Delta\beta_i^2}$ . Varying the detuning amplitude  $\Delta\beta_A$  from 0 to  $1 \text{ mm}^{-1}$ , we get the corresponding  $\sigma^2(\Delta\beta_i)$ , and meanwhile, we work out  $E_i^R$  by integrating the spectral density according to Eqs. (3) and (4). As shown in Fig. 3b, the experimental data exhibits excellent linearity in accordance with Eq. (5).

### Vibrational assistance

In state-of-the-art literature, the strong coupling to the the vibrational modes is believed to play an important role in energy transport<sup>25</sup>. The electronic coherence, vibronic coherence and vibrational coherence are found to live with different coherence time, which are 50–100fs, <500fs and >1000fs, respectively<sup>43,44</sup>. Our 20-mm-long photonic chip corresponds to an evolution time in the magnitude of 10ps, which goes beyond the above time scale. Still, it is interesting to investigate a vibrational assistance at the very early stage of evolution. We set an additional vibrational mode by an extra waveguide, with a vibrational coherence strength equal to the gap between the two lowest eigenstates of the 7-site Hamiltonian. As shown in Fig. 3c, the transport efficiency is clearly enhanced when coupling to the vibrational mode than without such a coupling. Note that this example uses a  $\Delta\beta_A$  of  $0.5 \text{ mm}^{-1}$ . For other noise amplitudes, the enhanced efficiency via vibrational assistance always exists. See more numerical details in the Supplementary Note 7.

Apart from the above issues, the issues of exciton transfer<sup>11</sup> and energy localisation<sup>45</sup> are also critical when discussing transport efficiencies. We illustrate the exciton transfer process inside FMO by numerically simulating the coherent light evolution in FMO-mimic waveguide array. By analyzing the most probable excited site when varying the propagation length, we see both large detunings of the site energy that induce strong disorders, and large-scale  $\Delta\beta$  noise that induce the Zeno effect, would enhance exciton localisation (see details in Supplementary Note 8). Furthermore, we show the disorder-induced enhancement of energy localisation by simulating the energy transport efficiency and the distribution of eigen-energy levels (see details in Supplementary Note 9).

### Quantum simulation experiment

In experiments, we have prepared four groups of samples in the coloured noise environment, having a range of  $\Delta\beta_A$  values 0, 0.1, 0.2, ...,  $1.0 \text{ mm}^{-1}$ . All samples have the noise settings that make a power spectral density consistent with the actual FMO complex. We inject the 810 nm vertically polarised coherent light into Waveguide 6 and measure the evolution patterns using a charge coupled device. We are kind of simulating the energy packet random walk using a coherent light because when there is only one walker, the quantum coherence effects are well simulated by a coherent light field<sup>46</sup>. We process the figures to read out the light intensity in the seven-site part  $I_{\text{FMO}}$  and the sink part  $I_{\text{sink}}$ . Then  $I_{\text{sink}}/(I_{\text{FMO}} + I_{\text{sink}})$  is worked out as the energy transport efficiency  $\eta$ . In Fig. 4a–d, the evolution patterns and the corresponding energy transport efficiencies for four samples in the same group of different  $\Delta\beta_A$  values are presented. The experimental results for all samples are provided in Supplementary Note 10.

We characterise the energy transport efficiencies for all samples (Fig. 4e) and show an optimal transport efficiency for all groups up to 96% when  $\Delta\beta_A$  increases up to  $0.5\text{--}0.6 \text{ mm}^{-1}$ , followed up by an efficiency droop when  $\Delta\beta_A$  further increases. Our experimental results based on the  $\Delta\beta$  photonic model show that the environmental noise can assist quantum transport, just as the name ENAQT<sup>11</sup> suggests. We show an optimal  $\Delta\beta_A$  that corresponds to an efficiency peak. This is consistent with our rich numerical analysis on the ENAQT effect (see Supplementary Note 11), where the optimal transport behaviour always occurs at an intermediate dephasing scale.

### Discussion

In summary, we have fully explored the capabilities of the  $\Delta\beta$  photonic model on quantum simulation of photosynthetic energy transport, with a case on the FMO complexes. By taking full advantages of the flexible arrangement of the array configuration in our three-dimensional photonic lattice, we manage a faithful layout of the coupling profile for the seven-site FMO complex. Meanwhile, the experimentally feasible  $\Delta\beta$  tuning enables us to set the base site energy for different BChls in FMO, and build the non-Markovian coloured noise that simulates the power spectral density of the actual FMO complex. Through these efforts, we experimentally demonstrate an optimal ENAQT transport in the photonic lattice. We also show that the  $\Delta\beta$  photonic model not only simulates ENAQT theories extensively studied during 2010s, but also can address many up-to-date interesting topics related to FMO energy transport such as the vibrational assistance.

Our quantum simulation experiment can be broadly adapted to simulating the photosynthesis processes in many other chlorophyll complexes, such as PE545, PE555, PC645, etc.<sup>47–49</sup>, given their protein structures, Hamiltonian matrices and noise spectrum. Our quantum simulation experiments can give insights on the scale of noise modulation for energy

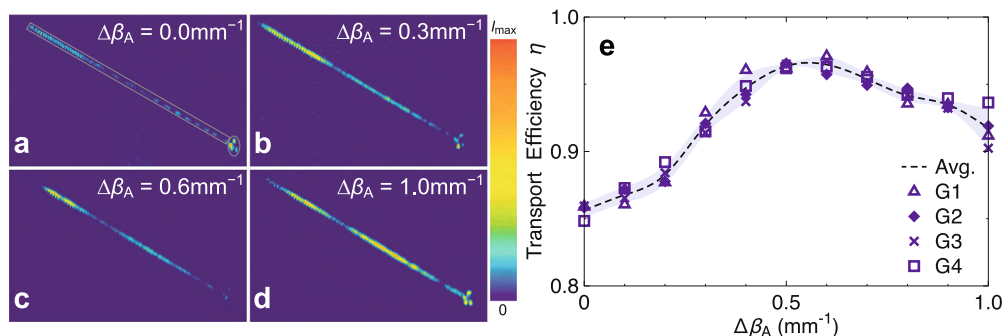


**Fig. 4 | Experimental transport patterns and the energy transport efficiency.** Three examples from the arrays formed with different  $\Delta\beta_A$  values show different energy transport efficiencies. The  $\Delta\beta_A$  values are  $0.0 \text{ mm}^{-1}$  for (a),  $0.3 \text{ mm}^{-1}$  for (b),  $0.6 \text{ mm}^{-1}$  for (c) and  $1.0 \text{ mm}^{-1}$  for (d). The zones for seven-site FMO complex and the sink are marked with an ellipse and a rectangle, respectively. The energy

transport efficiencies are given in the bottom-left of the figures. **e** The measured transport efficiencies for samples of different  $\Delta\beta_A$  values. The results for each individual sample and the averaged values are plotted in dots and a curve, respectively.

transport in those chlorophyll complexes. This study may inspire applications for bioscience<sup>50</sup>.

Our results demonstrate a powerful analog quantum simulator that can possibly be further applied to a rich diversity of researches on open quantum systems. We have noticed a recent work using digital quantum circuits to simulate the open quantum system dynamics<sup>51</sup>. They simulate four sites for FMO complex and require a long circuit depth, which will work on fault-tolerant devices in the future. The quantum simulation is indeed of a broad interest<sup>52</sup>, and strongly depends on the quantum hardware capabilities. Our integrated photonic chips have been used for various quantum simulation tasks<sup>53–55</sup> in the noisy intermediate-scale quantum era, and many can be further turned into practical modules for quantum information processing modules, such as Haar random matrix generation<sup>36</sup>, and on-chip quantum state preserving<sup>55</sup>, etc. This work of simulating FMO complexes essentially constructs the non-Markovian environments in photonic chips. Non-Markovian processes have been widely studied but still have many emerging applications, e.g., entanglement reactivation<sup>56</sup>, quantum storage<sup>57</sup>. In order to carry out innovative exploration of non-Markovianity and its applications, strict experimental conditions are always required, and our experimental endeavor provides a way out for implementing non-Markovianity. The approach with flexible Hamiltonian mapping and controllable introduction of noise on integrated photonics is useful and worthy of further exploration on quantum simulation and quantum information processing applications.

## Methods

### Sample preparation

All the waveguides are fabricated using the femtosecond laser direct writing technique. We direct a 513-nm femtosecond laser (upconverted from a pump laser of 10 W, 1026 nm, 290 fs pulse duration, 1 MHz repetition rate) into a spatial light modulator (SLM) to shape the laser pulse in the temporal and spatial domain. We then focus the pulse onto a pure borosilicate substrate with a 50X objective lens (numerical aperture: 0.55). Power and SLM compensation were processed to ensure waveguide uniformity<sup>37</sup>.

We have also characterised the quantitative control for  $\Delta\beta$  detunings in the photonic lattice. We write one waveguide using a base speed  $V_0$ , and the other one using a different speed  $V$  ( $V - V_0 = \Delta V$ ). In such a detuned directional coupler, the coupling mode method gives the effective coupling coefficient,  $C_{\text{eff}}$ , instead of  $C_0$ , the coupling coefficient for a normal directional coupler with  $\Delta V = 0$ .  $C_{\text{eff}}$  contains the detuning effect from  $\Delta\beta$  through:

$$C_{\text{eff}} = \sqrt{(\Delta\beta/2)^2 + C_0^2}. \quad (6)$$

Therefore, characterizing  $C_{\text{eff}}$  and  $C_0$  gives  $\Delta\beta$ . See details for the characterisation in Supplementary Note 2.

### Data availability

Data used for graphing in this paper are available from the corresponding author upon reasonable request.

Received: 6 May 2023; Accepted: 19 February 2024;

Published online: 11 March 2024

## References

- Engel, G. S. et al. Evidence for wavelike energy transfer through quantum coherence in photosynthetic systems. *Nature* **446**, 782–786 (2007).
- Lee, H., Cheng, Y. C. & Fleming, G. R. Coherence dynamics in photosynthesis: protein protection of excitonic coherence. *Science* **316**, 1462–1465 (2007).
- Collini, E. et al. Coherently wired light-harvesting in photosynthetic marine algae at ambient temperature. *Nature* **463**, 644 (2010).
- Panitchayangkoon, G. et al. Long-lived quantum coherence in photosynthetic complexes at physiological temperature. *Proc. Nat. Aca. Sci.* **107**, 12766–12770 (2010).
- Breuer, H.-P. & Petruccione, F. *The Theory of Open Quantum Systems*. Oxford University Press (2007).
- Mohseni, M., Robentrost, P., Lloyd, S. & Aspuru-Guzik, A. Environment-assisted quantum walks in photosynthetic energy transfer. *J. Chem. Phys.* **129**, 176106 (2008).
- Plenio, M. B. & Huelga, S. F. Dephasing-assisted transport: quantum networks and biomolecules. *N. J. Phys.* **10**, 113019 (2008).
- Caruso, F., Chin, A. W., Datta, A., Huelga, S. F. & Plenio, M. B. Highly efficient energy excitation transfer in light-harvesting complexes: The fundamental role of noise-assisted transport. *J. Chem. Phys.* **131**, 09B612 (2009).
- Caruso, F. Universally optimal noisy quantum walks on complex networks. *N. J. Phys.* **16**, 055015 (2014).
- Wu, J., Liu, F., Shen, Y., Cao, J. & Silbey, R. J. Efficient energy transfer in light-harvesting systems, I: optimal temperature, reorganization energy and spatial-temporal correlations. *N. J. Phys.* **12**, 105012 (2010).
- Rebentrost, P., Mohseni, M., Kassar, I., Lloyd, S. & Aspuru-Guzik, A. Environment-assisted quantum transport. *N. J. Phys.* **11**, 033003 (2009).
- Tao, M. J. et al. Coherent and incoherent theories for photosynthetic energy transfer. *Sci. Bull.* **65**, 318–328 (2020).
- Park, H. et al. Enhanced energy transport in genetically engineered excitonic networks. *Nat. Mater.* **15**, 211–216 (2016).

14. Scholes, G. D., Fleming, G. R., Olaya-Castro, A. & Van Grondelle, R. Lessons from nature about solar light harvesting. *Nat. Chem.* **3**, 763 (2011).
15. Lambert, N. et al. Quantum biology. *Nat. Phys.* **9**, 10–18 (2013).
16. Fenna, R. E. & Matthews, B. W. Chlorophyll arrangement in a bacteriochlorophyll protein from *Chlorobium limicola*. *Nature* **258**, 573–577 (1975).
17. Häse, F., Kreisbeck, C. & Aspuru-Guzik, A. Machine learning for quantum dynamics: deep learning of excitation energy transfer properties. *Chem. Sci.* **8**, 8419–8426 (2017).
18. Biggerstaff, D. N. et al. Enhancing quantum transport in a photonic network using controllable decoherence. *Nat. Commun.* **7**, 11282 (2016).
19. Harris, N. C. et al. Quantum transport simulations in a programmable nanophotonic processor. *Nat. Photonics* **11**, 447–452 (2017).
20. Potočnik, A. et al. Studying light-harvesting models with superconducting circuits. *Nat. Commun.* **9**, 904 (2018).
21. Wang, B. X. et al. Efficient quantum simulation of photosynthetic light harvesting. *npj Quantum Inf.* **4**, 52 (2018).
22. Tao, M. J. et al. Quantum simulation of clustered photosynthetic light harvesting in a superconducting quantum circuit. *Quantum Eng.* **2**, e53 (2020).
23. Maier, C. et al. Environment-Assisted Quantum Transport in a 10-qubit Network. *Phys. Rev. Lett.* **122**, 050501 (2019).
24. Tang, H. et al. TensorFlow solver for quantum PageRank in large-scale networks. *Sci. Bull.* **66**, 120–126 (2021).
25. Cao, J. et al. Quantum biology revisited. *Sci. Adv.* **6**, eaaz4888 (2020).
26. Thyryhaug, E. et al. Identification and characterization of diverse coherences in the Fenna-Matthews-Olson complex. *Nat. Chem.* **10**, 780–786 (2018).
27. Mančal, T. A decade with quantum coherence: How our past became classical and the future turned quantum. *Chem. Phys.* **532**, 110663 (2020).
28. Ishizaki, A. & Fleming, G. R. Insights into Photosynthetic Energy Transfer Gained from Free-Energy Structure: Coherent Transport, Incoherent Hopping, and Vibrational Assistance Revisited. *J. Phys. Chem. B* **125**, 3286–3295 (2021).
29. Wendling, M. et al. Electron-Vibrational Coupling in the Fenna-Matthews-Olson Complex of Prosthecochloris a estuarii Determined by Temperature-Dependent Absorption and Fluorescence Line-Narrowing Measurements. *J. Phys. Chem. B* **104**, 5825–5831 (2000).
30. Klinger, A., Lindorfer, D., Müh, F. & Renger, T. Normal mode analysis of spectral density of FMO trimers: Intra- and intermonomer energy transfer. *J. Chem. Phys.* **153**, 215103 (2020).
31. Ishizaki, A. & Fleming, G. R. Unified treatment of quantum coherent and incoherent hopping dynamics in electronic energy transfer: Reduced hierarchy equation approach. *J. Chem. Phys.* **130**, 234111 (2009).
32. Jang, S., Cheng, Y. C., Reichman, D. R. & Eaves, J. D. Theory of coherent resonance energy transfer. *J. Chem. Phys.* **129**, 101104 (2008).
33. Caruso, F., Crespi, A., Ciriolo, A. G., Sciarrino, F. & Osellame, R. Fast escape of a quantum walker from an integrated photonic maze. *Nat. Commun.* **7**, 11682 (2016).
34. Perez-Leija, A. et al. Endurance of quantum coherence due to particle indistinguishability in noisy quantum networks. *npj Quantum Inf.* **4**, 45 (2018).
35. Tang, H. et al. Experimental quantum stochastic walks simulating associative memory of Hopfield neural networks. *Phys. Rev. Appl.* **11**, 024020 (2019).
36. Tang, H. et al. Generating Haar-uniform randomness using stochastic quantum walks on a photonic chip. *Phys. Rev. Lett.* **128**, 050503 (2022).
37. Tang, H. et al. Experimental two-dimensional quantum walk on a photonic chip. *Sci. Adv.* **4**, eaat3174 (2018).
38. Tang, H. et al. Experimental quantum fast hitting on hexagonal graphs. *Nat. Photonics* **12**, 754–758 (2018).
39. Wang, Y. et al. Topologically protected polarization quantum entanglement on a photonic chip. *Chip* **1**, 100003 (2022).
40. Adolphs, J. & Renger, T. How proteins trigger excitation energy transfer in the FMO complex of green sulfur bacteria. *Biophys. J.* **91**, 2778–2797 (2006).
41. Hoyer, S., Sarovar, M. & Whaley, K. B. Limits of quantum speedup in photosynthetic light harvesting. *N. J. Phys.* **12**, 065041 (2010).
42. Chen, X. Y. et al. Global correlation and local information flows in controllable non-Markovian open quantum dynamics. *npj Quantum Inf.* **8**, 1–6 (2022).
43. Gelin, M. F., Borrelli, R. & Domcke, W. Origin of unexpectedly simple oscillatory responses in the excited-state dynamics of disordered molecular aggregates. *J. Phys. Chem. Lett.* **10**, 2806–2810 (2019).
44. Wang, L., Allodi, M. A. & Engel, G. S. Quantum coherences reveal excited-state dynamics in biophysical systems. *Nat. Rev. Chem.* **3**, 477–490 (2019).
45. Coates, A. R., Lovett, B. W. & Gauger, E. M. Localisation determines the optimal noise rate for quantum transport. *N. J. Phys.* **23**, 123014 (2021).
46. Jeong, H., Paternostro, M. & Kim, M. S. Simulation of quantum random walks using interference of classical field. *Phys. Rev. A* **69**, 012310 (2004).
47. Novoderezhkin, V. I., Doust, A. B., Curutchet, C., Schole, G. D. & van Grondelle, R. Excitation dynamics in phycoerythrin 545: modeling of steady-state spectra and transient absorption with modified redfield theory. *Biophys. J.* **99**, 344–352 (2010).
48. Chandrasekaran, S., Pothula, K. R. & Kleinekathöfer, U. Protein arrangement effects on the exciton dynamics in the PE555 complex. *J. Phys. Chem. B* **121**, 3228 (2016).
49. Zech, T., Mulet, R., Wellens, T. & Buchleitner, A. Centrosymmetry enhances quantum transport in disordered molecular networks. *N. J. Phys.* **16**, 055002 (2014).
50. Choi, E. H., Uhm, H. S. & Kaushik, N. K. Plasma bioscience and its application to medicine. *AAPPS Bull.* **31**, 10 (2021).
51. Hu, Z. X., Head-Marsden, K., Mazziotti, D. A., Narang, P. & Kais, S. A general quantum algorithm for open quantum dynamics demonstrated with the Fenna-Matthews-Olson complex. *Quantum* **6**, 726 (2022).
52. Georgescu, I. M., Ashhab, S. & Nori, F. Quantum simulation. *Rev. Mod. Phys.* **86**, 153–185 (2014).
53. Wang, Y. et al. Experimental parity-induced thermalization gap in disordered ring lattices. *Phys. Rev. Lett.* **122**, 013903 (2019).
54. Wang, Y. et al. Quantum simulation of particle pair creation near the event horizon. *Nat. Sci. Rev.* **7**, 1476–1484 (2020).
55. Tang, H. et al. Experimental quantum simulation of dynamic localization on curved photonic lattices. *Photonics Res.* **10**, 1430–1439 (2022).
56. Pirandola, S. et al. Environment-assisted bosonic quantum communications. *npj Quantum Inf.* **7**, 1–7 (2021).
57. Andersson, G., Suri, B., Guo, L., Aref, T. & Delsing, P. Non-exponential decay of a giant artificial atom. *Nat. Phys.* **15**, 1123–1127 (2019).
58. Ben-Shem, A., Frolow, F. & Nelson, N. Evolution of photosystem I - from symmetry through pseudosymmetry to asymmetry. *FEBS Lett.* **564**, 274–280 (2004).
59. Humphrey, W., Dalke, A. & Schulten, K. VMD - visual molecular dynamics. *J. Molec. Graph.* **14**, 33–38 (1996).

## Acknowledgements

The authors thank Prof. Roberto Osellame and Prof. Jian-Wei Pan for helpful discussions. The authors thank Dr. Stephan Hoyer for discussing on the Hamiltonian matrix for the FMO complex, thank Dr. Kiran Khosla for discussing on the open quantum system theories, thank Dr. Song Ke for

teaching the software on plotting the protein structure, and thank Prof. Fei Ma for sharing research works on vibrational assistance. This research was supported by the National Key R&D Program of China (Grant No. 2019YFA0706302, No. 2019YFA0308703, No. 2017YFA0303700); the National Natural Science Foundation of China (Grants No. 62235012, No. 11904299, No. 61734005, No. 11761141014, and No. 11690033, No. 12104299, and No. 12304342); Innovation Program for Quantum Science and Technology (Grants No. 2021ZD0301500, and No. 2021ZD0300700); Science and Technology Commission of Shanghai Municipality (STCSM) (Grants No. 20JC1416300, No. 2019SHZDZX01, No. 21ZR1432800, No. 22QA1404600), and the Shanghai Municipal Education Commission (SMEC) (2017-01-07-00-02-E00049). China Postdoctoral Science Foundation (Grants No. 2020M671091, No. 2021M692094, No. 2022T150415). X.-M.J. acknowledges additional support from a Shanghai talent program and support from Zhiyuan Innovative Research Center of Shanghai Jiao Tong University. H. T. acknowledges additional support from Yangyang Development Fund. MSK's work is supported by the UK Hub in Quantum Computing and Simulation with funding from UKRI EPSRC grant EP/T001062/1, a Samsung GRC grant, UK EPSRC grants EP/Y004752/1 and EP/W032643.

### Author contributions

H.T. and X.-W.S. contributed equally to this work. H.T. conceived the experiments. X.-W.S., H.T., Z.-Y.S., Z.F., and X.T. fabricated the femtosecond laser direct-writing chips with coloured noise sequence. X.-W.S. and T.-Y.W. performed the experiments. X.-W.S., H.-M.W., X.-Y.X. and J.G. collected and analyzed the data. H.T., X.-W.S. and R.S. conducted numerical simulations. X.-W.S., T.-S.H., and T.-Y.W. contributed to drawing the figures. H.T. and X.-W.S. developed the manuscript. M.S.K. and X.-M.J. contributed to the discussions of the results. X.-M.J. supervised the project.

### Competing interests

The authors declare no competing interests.

### Additional information

**Supplementary information** The online version contains supplementary material available at <https://doi.org/10.1038/s41534-024-00824-x>.

**Correspondence** and requests for materials should be addressed to Xian-Min Jin.

**Reprints and permissions information** is available at <http://www.nature.com/reprints>

**Publisher's note** Springer Nature remains neutral with regard to jurisdictional claims in published maps and institutional affiliations.

**Open Access** This article is licensed under a Creative Commons Attribution 4.0 International License, which permits use, sharing, adaptation, distribution and reproduction in any medium or format, as long as you give appropriate credit to the original author(s) and the source, provide a link to the Creative Commons licence, and indicate if changes were made. The images or other third party material in this article are included in the article's Creative Commons licence, unless indicated otherwise in a credit line to the material. If material is not included in the article's Creative Commons licence and your intended use is not permitted by statutory regulation or exceeds the permitted use, you will need to obtain permission directly from the copyright holder. To view a copy of this licence, visit <http://creativecommons.org/licenses/by/4.0/>.

© The Author(s) 2024